Published in final edited form as:
J Am Chem Soc. 2012 December 5; 134(48): 19731–19738. doi:10.1021/ja308049u.

Dissection of Hydrogen Bond Interaction Network around an Iron-sulfur Cluster by Site-specific Isotope Labeling of Hyperthermophilic Archaeal Rieske-type Ferredoxin

Toshio Iwasaki[*,†], **Risako Fukazawa**[†], **Yoshiharu Miyajima-Nakano**[†], **Amgalanbaatar Baldansuren**[‡], **Shinichi Matsushita**[†], **Myat T. Lin**[§], **Robert B. Gennis**[§], **Kazuya Hasegawa**[¶], **Takashi Kumasaka**[¶], and **Sergei A. Dikanov**[*,‡]

[†]Department of Biochemistry and Molecular Biology, Nippon Medical School, Sendagi, Tokyo 113-8602, Japan

[‡]Department of Veterinary Clinical Medicine, University of Illinois at Urbana-Champaign, Urbana, Illinois 61801, United States

[§]Department of Biochemistry, University of Illinois at Urbana-Champaign, Urbana, Illinois 61801, United States

[¶]Japan Synchrotron Radiation Research Institute (SPring-8/JASRI), Sayo, Hyogo 679-5198, Japan

Abstract

The electronic structure and geometry of redox-active metal cofactors in proteins are tuned by the pattern of hydrogen bonding with the backbone peptide matrix. In this study we developed a method for selective amino acid labeling of a hyper-thermophilic archaeal metalloprotein with engineered *Escherichia coli* auxotroph strains, and applied this to resolve the hydrogen bond interactions with the reduced Rieske-type [2Fe-2S] cluster by two-dimensional pulsed electron spin resonance (EPR) technique. Because deep electron spin-echo envelope modulation of two histidine $^{14}N_{\delta}$ ligands of the cluster decreased non-coordinating ^{15}N signal intensities via the cross-suppression effect, an inverse labeling strategy was employed in which ^{14}N amino acid-labeled archaeal Rieske-type ferredoxin samples were examined in an ^{15}N-protein background. This has directly identified Lys45 N_{α} as providing the major pathway for the transfer of unpaired electron spin density from the reduced cluster by a “through-bond” mechanism. All other backbone peptide nitrogens interact more weakly with the reduced cluster. The extension of this approach will allow visualizing the three-dimensional landscape of preferred pathways for the transfer of unpaired spin density from a paramagnetic metal center onto the protein frame, and will discriminate specific interactions by a “through-bond” mechanism from interactions which are “through-space” in various metalloproteins.

Introduction

Metal-based redox cofactors, such as iron-sulfur clusters, heme, copper, non-heme iron, manganese, and molybdenum ions, are essential to sustain all life forms, and some of them

Corresponding Author tiwasaki@nms.ac.jp; dikanov@illinois.edu.

Author Contributions
All authors have given approval to the final version of the manuscript.

The authors declare no competing financial interest.

Supporting Information. Table S1. This material is available free of charge via the Internet at http://pubs.acs.org.

can be finely tuned to catalyze some of the most difficult reactions in biology.[1–7] Although these cofactors are often bound to the protein matrix with the (mostly) same ligand set within each class, they can exhibit vastly different redox properties and functions. This demonstrates that accumulative natural mutations of the local non-coordinating residues around the metal binding site can modulate its electronic structure and geometry. Of particular fundamental interest is how the protein matrix achieves the appropriate setting of the metal binding site for the distinctive specificity and reactivity *in vivo*[1–3,8–11]

The interactions of the cofactors with the polypeptide matrix can be through covalent bonds (ligation) or hydrogen bonds, or can be due to non-bonding interactions, including, but not exclusively, electrostatic interactions. Among various aspects of metalloprotein structure, reorganization of a metal ligand(s) and/or hydrogen-bonding network around a redox-active site(s) is often utilized in modulating the redox potentials (E_m) and functionalities in nature, as in iron-sulfur proteins,[2,12–15] cupredoxins,[10,16] and cytochromes;[11] other strategies in myoglobins and cytochromes include changes in the hydrophobicity[11,17,18] and possibly protein-induced distortion of heme-porphyrin structure,[19] which can greatly influence on the heme E_m and electronic properties (although the solvent effects have shown rather minimal influence in cupredoxins[10]). The outlook for these structural variations is that subtle interactions outside the primary coordination sphere are exclusively used to attain the required E_m and functions in each metalloprotein family. X-ray crystallography is an indispensible tool to define the geometric relationships of residues around a metal cofactor-binding site, but cannot by itself define the strength of the interactions, particularly with putative hydrogen bonds around the transition metal ion sites. A fundamental understanding of the relationship between the structure and redox chemistry of metalloproteins would not only provide deeper insights into the structure and mechanism of proteins, but also facilitate the rational design of proteins with desirable chemical properties for biotechnological and pharmaceutical applications.

Protein-associated iron-sulfur clusters and their derivative cofactors play remarkably versatile roles *in vivo*.[2,9,20,21] Of these, Rieske-type [2Fe-2S](His)$_2$(Cys)$_2$ clusters are involved in various electron transfer reactions such as photosynthesis, aerobic respiration, and biodegradation of various alkene and aromatic compounds.[22–25] The Rieske-type clusters exhibit a wide range of the E_m relevant to the *in vivo* functions. The E_m's span from about −150 to −50 mV for a low-potential cluster in archaeal and bacterial Rieske-type ferredoxins, to about +150 to +490 mV for a high-potential cluster in Rieske proteins from quinol-oxidizing cytochrome bc_1/b_6f complexes.[12,23] This demonstrates that accumulative natural mutations of the local non-coordinating residues around the cluster binding site can modulate its electronic structure and geometry. Previous protein structural and electrochemical studies indicate that a lower potential cluster tends to have less extensive hydrogen bonding network around the Rieske-type cluster.[12–14,26,27] The (N/O)-H···S hydrogen bond network around biological iron-sulfur clusters is one of critical factors in modulating their redox properties. For example, a short N-H···S hydrogen bond would lead to more efficient electron delocalization and stabilization of the negative charge in the reduced, electron-rich state, thereby preferentially increasing the E_m of the cluster, whereas the deletion of a direct hydrogen bond to a sulfur ligand can lower the cluster E_m by increasing the electron density on this ligand. The theoretical analysis further suggests that the distribution of negatively charged residues around the cluster modulates the pH dependence of cluster E_m in the low-potential homologs.[28]

Pulsed EPR techniques such as electron spin-echo envelope modulation (ESEEM) and electron-nuclear double resonance (ENDOR) probe specific interaction between electron spin of a paramagnetic center and nuclear spin of its protein frame.[29–31] In case of the Rieske-type [2Fe-2S](His)$_2$(Cys)$_2$ cluster system, strong antiferromagnetic coupling

between the electron spins of the two irons produces an EPR-silent (S=0) ground state in the oxidized Fe^{3+}-Fe^{3+} form, and a paramagnetic S=1/2 ground state in the reduced Fe^{3+}-Fe^{2+} form. Direct interaction of the reduced Rieske-type cluster with a particular protein residue by either covalent or hydrogen bonding can result in the distribution of unpaired electron spin density onto the protein matrix. For N-H•••S hydrogen bonds with the cluster, for example, this "through-bond" transfer of unpaired spin density to the nitrogen nucleus via the overlapped electronic orbitals can be probed experimentally by pulsed EPR.[32] For this purpose, the two-dimensional, four-pulse ESEEM (also called hyperfine sublevel correlation, HYSCORE) technique has become a powerful tool. Using this technique, one can quantify the nuclear frequencies of interest from electron spin m_S=+1/2 and −1/2 manifolds belonging to the same nucleus, such as ^{1}H, ^{2}H, ^{14}N, and ^{15}N, which are resolved as non-diagonal cross-peak coordinates.[29,32,33] In conjunction with a protein structure determined by X-ray crystallography, these data can be used to describe local *spatial* and *electronic* structures around the cluster which influence the metalloenzyme functionalities and reactivities.

X-band ^{14}N HYSCORE spectra of the reduced Rieske-type clusters are dominated by two histidine N_δ ligands with hyperfine couplings ~4–5 MHz.[32] Additionally, one or a few more non-coordinating ^{14}N around the reduced cluster can also produce much less intense lines in the ^{14}N spectra, as a result of the nuclear quadrupole interaction influence.[32] The latter features are better pronounced in the (++) quadrant of the spectra of the proteins uniformly labeled with ^{15}N (nuclear spin I=1/2, no quadrupole moment). These signals can potentially provide information about *all* ^{15}N nuclei involved in the measurable magnetic interactions with the unpaired electron spin of the reduced cluster.[33] In initial studies, two resolved splittings of 1.0–1.2 MHz and 0.3–0.5 MHz from non-coodinating ^{15}N cross-features were tentatively assigned to peptide nitrogen(s) (N_p) and remote N_ε of two histidine imidazole ligands, respectively.[33,34] However, the spectral variations of cross-peak intensities and lineshapes of non-coordinating ^{15}N signals in different Rieske-type proteins indicate that such earlier interpretations were oversimplified. The aggregate weakly coupled ^{15}N signals have additional contributions from multiple $^{15}N_p$ nuclei around the reduced cluster with non-equivalent couplings.[35] Since these interactions can contribute to tuning the properties of the Rieske-type [2Fe-2S] cluster, further resolution of these interactions has motivated the current study.

Belonging to the low-potential class of the Rieske-type ferredoxin family, a new tractable model protein of interest is the hyperthermostable archaeal Rieske-type ferredoxin (ARF) from *Sulfolobus solataricus* strain P1 ($E_{m,7}$ ~ −60 mV), which is homologous to oxygenase-associated Rieske-type ferredoxins (DDBJ/EMBL/GenBank code AB047031).[36] Recombinant ARF has been overproduced in *Escherichia coli* and can be obtained in appropriate forms for uniformly stable isotope labeling, site-directed ligand mutagenesis, and various spectroscopic analyses.[36–38] The dithionite-reduced Rieske-type [2Fe-2S] cluster in ARF is characterized by the anisotropic EPR spectrum, as a result of a rhombic g-tensor ($g_{z,y,x}$=2.02, 1.90, 1.81).[36] Orientation-selective HYSCORE spectra of unlabeled (^{14}N(N/A))[32] and uniformly ^{15}N-labeled[35] ARF have been analyzed, and the lines from weakly coupled (non-coordinating) ^{15}N of ARF showed lower intensities than those of the corresponding ^{15}N signals of the high-potential Rieske protein homologs. Recent crystal structure of ARF refined to 1.85-Å resolution[39] indicates the involvement of four possible amino acid residues in N-H•••S hydrogen bond network with the sulfur atoms of the archaeal Rieske-type [2Fe-2S](His)$_2$(Cys)$_2$ cluster: Lys45 N_α-S^b (N-S distance, 3.28 Å), His64 N_α-S^b (N-S distance, 3.57 Å), His44 N_α-Cys42 S_γ (3.46 Å), and Tyr66 N_α-S^b (3.53 Å) (Fig. 1). The number of possible N-H•••S hydrogen bonds around the cluster is less than those found for the high-potential homologs.[39b]

In the current work, we demonstrate a strategy utilizing site-specific amino acid labeling and pulsed EPR spectroscopy to compare two predicted N-H•••S hydrogen bonds between backbone peptide nitrogens and the reduced Rieske-type [2Fe-2S] cluster of *S. solfataricus* ARF. This spectroscopic approach provides additional physicochemical parameters to characterize the through-bond interactions between the cluster and the protein matrix.

Experimental Section

Preparation of new auxotroph strains

Amino acid-selective isotope labeling is an extremely powerful method to elucidate specific contributions of particular residues in the reaction mechanisms and/or folding of a target protein by magnetic resonance and vibrational spectroscopies, often aided by the X-ray crystal structure. One of the most convenient and cost-effective procedures for selective isotope labeling of proteins is to employ amino acid auxotrophic bacteria as the host strains for the overproduction of target proteins. However, no suitable auxotrophic strains are commercially available for high-level expression of the foreign genes coding for metalloenzymes from extremophilic bacteria and archaea, because (i) their high-level expression, *e.g.*, in *Escherichia coli*, often requires extra copies of tRNA genes for the cognate rare codons and (ii) specific growth conditions must be set for effective overproduction of holoproteins in a form suitable for biophysical studies.[33,36]

To overcome these problems, Lin *et al.*[40] have reported the construction of a set of cost-effective, high-yield auxotrophs in commonly used *E. coli* expression strain C43(DE3) (Table 1). Of the amino acids selected for site-specific labeling in this study, L-tyrosine is biosynthesized by the pathways involving transaminases encoded by *aspC* and *tyrB* genes in *E. coli*.[41] Although it was possible to delete the *aspC* gene from the chromosomes of *E. coli* C43(DE3) and BL21(DE3) strains (Fig. 2, steps 1–4), the previous multiple attempts to replace the cognate *tyrB* locus of the C43(DE3) strain with an antibiotic resistance cassette have not been successful, for reasons that are not clear.[40] In this study we could successfully knock out the both *aspC* and *tyrB* genes from the chromosome of *E. coli* BL21-CodonPlus(DE3)-RIL strain (Stratagene) with a set of polymerase chain reaction (PCR) primers listed in Table S1, and the resulting new BL21(DE3) auxotroph is applicable to L-tyrosine (and probably L-phenylalanine)[41] labeling (Table 1, Fig. 2). It should be added that we were not able to delete the *tyrB* locus in *E. coli* C43(DE3) strain with these PCR primers (not shown), suggesting chromosomal DNA sequence differences around the *tyrB* region between the BL21(DE3) and C43(DE3) expression strains.

We adapted some of these auxotroph strains by incorporation of a pACYC-based plasmid harboring tRNA genes (*argU*, *ileY*, and leuW) for the *E. coli* rare codons (Agilent Technologies) (step 5 in Fig. 2), and developed heterologous expression procedures suitable for site-specific isotope labeling of archaeal iron-sulfur proteins (see below).

Preparation of site-specifically labeled ARF samples for pulsed EPR

The *arf* gene coding for the hyperthermostable archaeal Rieske-type [2Fe-2S](His)$_2$(Cys)$_2$ ferredoxin from *Sulfolobus solfataricus* strain P1 (DSM 1616) has been cloned and sequenced (DDBJ/EMBL/GenBank code AB047031) and heterologously overexpressed in *E. coli* BL21-CodonPlus(DE3)-RIL strain (Stratagene) using a pET28aARF vector (based on a pET28a His-tag expression vector, Novagen) and purified.[36] The structure of the recombinant ARF has been determined and refined at 1.85-Å resolution (to be published),[39] and is depicted with PyMOL <http://www.pymol.org> (Fig. 1).

For preparation of the uniformly ^{15}N-labeled ARF sample, the pET28aARF vector[36] was transformed into the host strain, *E. coli* BL21-CodonPlus(DE3)-RIL (Stratagene), and the

transformants were grown overnight at 25 °C in 1L culture (in 2L-flask) of the CHL-^{15}N (~97 atm%) medium (Chlorella Industry Co. Ltd., Fukuoka, Japan) containing 50 mg/L kanamycin, 0.2 mM $FeCl_3$, and the recombinant holoprotein was overproduced with 0.25 g/L $MgSO_4$•7 H_2O, 0.5 g/L Algal ^{15}N(98.7–99.2%)-Amino Acid Mix (Chlorella Industry Co. Ltd., Fukuoka, Japan) and 1 mM IPTG for ~18–22 h at 25 °C.[44] This system was suitable for heterologous overproduction of the uniformly ^{15}N-labeled iron-sulfur holoproteins by employing the combination of a pET28a vector (Novagen) plus *E. coli* BL21-CodonPlus(DE3)-RIL host strain (Stratagene) system.[44] The cells were pelleted at 4 °C by centrifugation, and stored at −80 °C until use.

For preparation of the selectively Lys $^{15}N_\alpha$- and Cys $^{15}N_\alpha$-labeled ARF samples [on the ^{14}N(N/A)-protein background; see Fig. 3], the *E. coli* C43(DE3) auxotroph strains ML40K1[40] and YM154 (Table 1 and Fig. 2, step 5), respectively, were used as parent cells for heterologous overexpression of the *S. solfataricus arf* gene. Because of the removal of the original resistance cassette during the construction of new auxotroph strains (Fig. 2, step 4), the knock-out of each target chromosomal gene in these host cells was verified by PCR prior to use (Table S1). In addition, our previous heterologous expression strategy developed for site-specific labeling of bacterial [2Fe-2S] ferredoxin[40] did not work with this archaeal metalloprotein, for which we found the absolute requirement of a much longer-term cultivation for effective heterologous production of a *holoprotein* form in *E. coli* C43(DE3) and BL21(DE3) strains. Therefore, we set the specific growth conditions for effective site-specific labeling of the ARF holoprotein in a form suitable for biophysical studies as described below.

The pET28aARF vector[36] was transformed into each strain of the resulting auxotrophs, and the transformants were grown overnight at 25 °C in a total of 2 L culture (using two 2 L-flasks, each containing 1L culture medium) of the Luria-Bertani medium containing 25 mg/L kanamycin, 17 mg/L chloramphenicol, and 0.2 mM $FeCl_3$. The cells were harvested at 10 °C by centrifugation, and the resulting cell pellet was subsequently inoculated into a total of 2 L culture (using two 2L-flasks, each containing 1L culture medium) of the freshly prepared, nonlabeled CHL medium (Chlorella Industry Co. Ltd., Fukuoka, Japan) containing 25 mg/L kanamycin, 17 mg/L chloramphenicol, 0.2 mM $FeCl_3$, 0.25 g/L $MgSO_4$•7 H_2O, and 0.5 g/L nonlabeled Algal Amino Acid Mix (Chlorella Industry Co. Ltd., Fukuoka, Japan), in the presence of extra unlabeled L-amino acids [0.23 g/L L-isoleucine, 0.25 g/L L-valine, 0.1 g/L L-histidine, 0.4 g/L L-arginine, 0.25 g/L L-methionine, and 0.65 g/L L-glutamic acid for selective Lys $^{15}N_\alpha$ labeling work; and 0.5 g/L L-alanine, 0.65 g/L L-glutamic acid, 0.55 g/L glycine and 2.1 g/L L-serine, and 0.025–0.05 g/L L-cysteine for selective Cys $^{15}N_\alpha$ labeling work] (purchased from either Wako Pure Chemicals, Nacalai Tesque, or Sigma Chemicals). The cells were grown in this culture in the presence of 1 mM IPTG for 5 h at 25 °C, and then further allowed to be grown continuously for another 44–50 h at 25 °C in the presence of ~0.05 g/L L-cysteine labeled at the $^{15}N_\alpha$ position (Cambridge Isotope Laboratories, Inc., Andover, MA) or 0.42 g/L L-lysine labeled at the $^{15}N_\alpha$ position (Cambridge Isotope Laboratories, Inc., Andover, MA). The cells were pelleted at 4 °C by centrifugation and stored at −80 °C until use.

For preparation of the selectively ^{14}N(N/A) Lys- and ^{14}N(N/A) Tyr-labeled ARF samples [on the ^{15}N-protein background], *E. coli* auxotrophs C43(DE3) strain ML40K1 and BL21(DE3) strain RF4RIL (Table 1 and Fig. 2, step 5), respectively, were used as parent cells for heterologous overexpression of the *S. solfataricus arf* gene. The knock-out of each target chromosomal gene was verified by PCR prior to use (Table S1). The pET28aARF vector[36] was transformed into each host auxotroph strain, and the transformants were grown overnight at 25 °C in 1 L culture (in 2 L-flask) of the CHL-15N (~97 atm%) medium (Chlorella Industry Co. Ltd., Fukuoka, Japan) containing 25 mg/L kanamycin, 17 mg/L

chloramphenicol, 0.2 mM $FeCl_3$, 0.25 g/L $MgSO_4$•7 H_2O, and 0.5 g/L Algal ^{15}N(98.7–99.2%)-Amino Acid Mix (Chlorella Industry Co. Ltd., Fukuoka, Japan). The cells were harvested at 10 °C by centrifugation, and the resulting cell pellet was subsequently inoculated into a total of 2 L culture (using two 2L-flasks, each containing 1L culture medium) of the freshly prepared, CHL-^{15}N (~97 atm%) medium (Chlorella Industry Co. Ltd., Fukuoka, Japan) containing 25 mg/L kanamycin, 17 mg/L chloramphenicol, 0.2 mM $FeCl_3$, 0.25 g/L $MgSO_4$•7 H_2O, and 0.5 g/L Algal ^{15}N(98.7–99.2%)-Amino Acid Mix (Chlorella Industry Co. Ltd., Fukuoka, Japan). The cells were grown in this culture in the presence of 1 mM IPTG for 5 h at 25 °C, and then further allowed to be grown continuously for another 48–50 h at 25 °C in the presence of ~0.183 g/L unlabeled L-tyrosine (Nacalai Tesque, Japan) or 0.42 g/L unlabeled L-lysine (Sigma Chemicals). The cells were pelleted at 4 °C by centrifugation.

Each ARF holoprotein sample was purified as reported previously for the unlabeled (^{14}N(N/A)) protein,[36] and concentrated with Centriprep-10 and Microcon-YM10 apparatus (Amicon) to ~0.5–1 mM in the presence of 1 M NaCl. For high-resolution pulsed EPR analysis, the resulting ARF samples (~0.5–1 mM, ~15–40 μL) were subsequently reduced with sodium dithionite under continuous flow of dry argon gas inside suprasil quartz EPR tubes (Wilmad) prior sealing, rapidly frozen in liquid nitrogen, and shipped in the frozen state in dry ice by international priority delivery service from Tokyo, Japan, to Urbana, U.S.A.

Pulsed EPR related methods

The pulsed EPR experiments were carried out at 10 K using an X-band Bruker ELEXSYS E580 spectrometer equipped with Oxford CF 935 cryostats.[32,35,44] The two-dimensional, four-pulse experiment ($\pi/2$-τ-$\pi/2$-t_1-π-t_2-$\pi/2$-τ-*echo*, also called HYSCORE) was employed with appropriate phase-cycling schemes to eliminate unwanted features from the experimental echo envelopes. The intensity of the echo after the fourth pulse was measured with t_2 and t_1 varied and constant τ. The length of a $\pi/2$ pulse was nominally 16 ns and a π pulse 32 ns. HYSCORE data were collected in the form of 2D time-domain patterns containing 256×256 points with steps of 20 or 32 ns. Spectral processing of ESEEM patterns, including subtraction of relaxation decay (fitting by polynoms of 3–4 degree), apodization (Hamming window), zero filling, and fast Fourier transformation (FT), was performed using Bruker WIN-EPR software.

Results and Discussion

$^{14,15}N$ HYSCORE analysis of ^{15}N-amino acid labeled ARF on the ^{14}N(N/A)-protein background

For this study we prepared several amino acid specifically nitrogen-labeled ARF samples by using the amino acid auxotroph strains of *E. coli* C43(DE3)[40] and BL21(DE3) derivatives harboring a pACYC-based plasmid harboring tRNA genes (*argU*, *ileY*, and leuW) for the *E. coli* rare codons (Agilent Technologies) (step 5 in Fig. 2), as described under the Experimental Section. These proteins were then subjected to experimentally dissect and identify the non-coordinating residue(s) directly interacting with the reduced cluster by a "through-bond" mechanism.

We initially prepared several different batches of selectively ^{15}N amino acid-labeled ARF samples on the ^{14}N(N/A)-protein background. Such samples had been presumed as suitable for resolution of individual non-coordinating $^{15}N_p$ signals by ^{15}N HYSCORE.[40] In the case of Rieske-type proteins, however, none of them unexpectedly showed any recognizable ^{15}N hyperfine splittings (Fig. 3). The resulting spectra were exclusively dominated by ^{14}N features mainly from the two hisidine N_δ ligands, similar to the spectra reported for

unlabeled (^{14}N(N/A)) ARF.[32] This suggests that deep ESEEM from the two coordinating $^{14}N_{\delta(His)}$ of the Rieske-type cluster decreases the non-coordinating ^{15}N signal intensities via the cross-suppression mechanism,[45] thus leaving only vague $^{15}N_p$ features in the (++) quadrant (Fig. 3).

^{14,15}N HYSCORE analysis of ^{14}N(N/A)-amino acid labeled ARF on the ^{15}N-protein background

To eliminate this problem, we prepared selectively ^{14}N(N/A) L-tyrosine and L-lysine labeled ARF samples on the ^{15}N-protein background, such that the two histidine ligands as well as other non-target amino acid residues around the cluster are exclusively ^{15}N labeled (Fig. 4). L-Tyrosine and L-lysine were selected in the light of putative N-H$^{\bullet\bullet\bullet}$S hydrogen bond network around the Rieske-type cluster in the ARF structure[39b] (Fig. 1). In both samples, the cross-features produced by different types of ^{15}N could be successfully resolved in the orientation-selected HYSCORE spectra measured at different field positions of the EPR line. In the (+−) quadrant, two pairs of cross-peaks with a contour parallel to the diagonal line are detected, which are attributed to the two histidine nitrogen ligands to the reduced cluster, $^{15}N_{\delta}1$ and $^{15}N_{\delta}2$. These have hyperfine couplings of the order 6 and 8 MHz, respectively, with predominantly isotropic character. These features are identical to those reported for uniformly ^{15}N-labeled ARF, showing the hyperfine tensors in the axial approximation of a=6.5 and T=1.5 MHz for $^{15}N_{\delta}1$ (presumably His44 N_{δ}), and a=7.9 MHz and T=1.6 MHz for $^{15}N_{\delta}2$ (presumably His64 N_{δ}).[35] These tensors are very similar to those reported for other Rieske-type proteins by the orientation-selected ^{15}N Q-band ENDOR.[46] These samples do not exhibit any $^{14}N_{\delta(His)}$ cross-features in the (+−) quadrant, indicating negligible (or limited) scrambling of input ^{14}N(N/A) L-amino acid.

Significant variations in HYSCORE spectra of the two samples are observed in the (++) quadrant (Fig. 5). For ^{14}N L-tyrosine labeled ARF, two superimposed pairs of the cross-features are located symmetrically around the diagonal point with ^{15}N Zeeman frequency, and clearly resolved in the “single-crystal like spectra” recorded at the low- and high-field edges near g_z and g_x values. These features define the approximate ^{15}N splittings of 1.04 MHz and 0.43 MHz near g_z, and 1.12 and 0.49 MHz near g_x (Table 2). Similar splittings have been observed in the corresponding uniformly ^{15}N-labeled ARF spectra.[35] Simultaneously, the input ^{14}N L-tyrosine gave a narrow, “inverse” ^{15}N splitting of ~0.2 MHz in the ^{15}N spectra recorded near g_y (Fig. 6B,D), but did not produce any new ^{14}N lines because the splitting is too small to be observable in the ^{14}N spectra (Fig. 4A).

In stark contrast, the spectra of ^{14}N L-lysine labeled ARF showed simpler cross-features with splittings of 0.42 MHz near g_z, and 0.50 MHz near g_x (Figs. 5,6 and Table 2). The larger ^{15}N splitting, with the isotropic hyperfine coupling a=1.03 MHz observed in the uniformly ^{15}N-labeled[35] and ^{14}N L-tyrosine labeled ARF, is missing (Fig. 6E–G, Table 2). Conversely, the input ^{14}N L-lysine clearly gave ^{14}N cross-peaks in the spectra of ^{14}N L-lysine labeled ARF (Figs. 4,5), at the equivalent positions as previously observed for the peptide nitrogen cross-peaks (**P1**) in unlabeled (^{14}N(N/A)) ARF spectra.[32]

Taken together, the results demonstrate that the largest splitting, with an isotropic coupling a=1.03 MHz in the (++) quadrant of the ^{15}N spectra of ARF (Table 2), is predominantly contributed from the single peptide nitrogen Lys45 N_{α}, which also gives the P1 (**N_p1**) cross-peaks in the corresponding 14N spectra.[32] Notably, Lys45 N_{α} is located near S^b (with the shortest N_{α}-S^b distance of 3.28 Å), in a reasonable orientation for an N_{α}-H$^{\bullet\bullet\bullet}S^b$ hydrogen bond (Fig. 1). Thus, Lys45 N_{α} provides the major pathway for unpaired spin density transfer from the reduced cluster via overlapped orbitals, i.e., by a “through-bond” mechanism. A similar conclusion was reached from a more qualitative theoretical analysis of a high-potential Rieske protein domain from *Rhodobacter sphaeroides*.[34] Thus, this particular

chemical bond interaction affecting the ground-state electronic structure of the reduced cluster is probably conserved among the Rieske-type protein scaffolds, and is not linked specifically to differences in cluster E_m. On the other hand, although Tyr66 N_α is located also in the range of a possible hydrogen bond distance from the cluster (with a slightly longer N_α-S^b distance of 3.53 Å, Fig. 1), the interaction with Tyr66 N_α appears to be predominantly an electron-nuclear dipole interaction (i.e. mainly by a "through-space" effect), and may be much weaker. Thus, although Lys45 N_α and Tyr66 N_α exhibit a near *pseudo*-two fold symmetry relative to the cluster plane, the unpaired electron spin density distribution over the polypeptide frame around the reduced cluster is highly asymmetric. The reason for this extreme asymmetry is not apparent and will require computational approaches to clarify.

Conclusions

The electronic structure and geometry of clusters in the Rieske-type proteins are fine-tuned by the pattern of hydrogen bonding with the backbone peptide matrix. The current work has demonstrated that the interaction between the Rieske-type [2Fe-2S] cluster with Lys45 N_α is dominant in ARF, but there are other interactions indicated with non-coordinating residues. Further resolution of individual non-coordinating backbone peptide ^{15}N signals with splittings in the range ~0.4–0.5 MHz or less (Fig. 5B) will require an extension of the current labeling strategy, with the systematic *double* labeling of ^{15}N histidine *plus* ^{15}N amino acid with an ^{14}N(N/A)-protein background. This will bypass the cross-suppression[45] of the non-coordinating ^{15}N signals by the otherwise predominant $^{14}N_\delta$ cross-peaks from two histidine ligands in the Rieske-type cluster system (see Fig. 3). By defining which interactions result in the transfer of unpaired electron spin density to the protein frame quantitatively with reference to the atomic coordinates, the application of the experimental approach described in this work provides physico-chemical parameters to characterize the through-bond interactions with the protein matrix which modulate the electronic structure, geometry, and reactivity of protein-associated, paramagnetic iron-sulfur cluster systems.[2,3,8,9]

It should be noted that chemical and biological activity of metalloenzymes depends upon the association of the metallo-cofactor and the protein matrix moiety. The present strategy of applying 2D pulsed EPR techniques in conjunction with selective isotope labeling should be applicable to probe the primary coordination sphere and the outer sphere through-bond and other interactions with paramagnetic active site metal centers in various metalloproteins and model peptides, which are usually obscured by multiple weak electron-nuclear interactions[32] and/or can be cross-suppressed by strongly coupled histidine imidazole ^{14}N ligands when exist.[45] This will not only help to reveal hidden structural features and possibly dynamics of active site residues during catalysis that may be inaccessible from other techniques, but also can contribute to develop and verify strategies for designing and engineering new metalloenzymes for biotechnological and pharmaceutical applications.

Supplementary Material

Refer to Web version on PubMed Central for supplementary material.

Acknowledgments

This investigation was supported in part by the International Collaborations in Chemistry Grant from JSPS (T.I.) and NSF (CHE-1026541 to S.A.D.), the JSPS Grant-in-aid 24659202 (T.I.), the DE-FG02-87ER13716 (R.B.G.) and DE-FG02-08ER15960 (S.A.D.) Grants from US DOE, NIH & NIGMS Roadmap Initiative (R01GM075937), and NIH grant GM062954 (S.A.D.).

References

1. Holm RH, Kennepohl P, Solomon EI. Chem Rev. 1996; 96:2239. [PubMed: 11848828]
2. Beinert H, Holm RH, Münck E. Science. 1997; 277:653. [PubMed: 9235882]
3. Solomon EI, Xie X, Dey A. Chem Soc Rev. 2008; 37:623. [PubMed: 18362972]
4. Rees DC. Annu Rev Biochem. 2002; 71:221. [PubMed: 12045096]
5. Thauer RK, Kaster AK, Goenrich M, Schick M, Hiromoto T, Shima S. Annu Rev Biochem. 2010; 79:507. [PubMed: 20235826]
6. Peters JW, Broderick JB. Annu Rev Biochem. 2012; 81:429. [PubMed: 22482905]
7. Hosler JP, Ferguson-Miller S, Mills DA. Annu Rev Biochem. 2006; 75:165. [PubMed: 16756489]
8. Lin IJ, Gebel EB, Machonkin TE, Westler WM, Markley JL. Proc Natl Acad Sci USA. 2005; 102:14581. [PubMed: 16199518]
9. Machonkin TE, Westler WM, Markley JL. Inorg Chem. 2005; 44:779. [PubMed: 15859246]
10. Marshall NM, Garner DK, Wilson TD, Gao YG, Robinson H, Nilges MJ, Lu Y. Nature. 2009; 462:113. [PubMed: 19890331]
11. Dolla A, Blanchard L, Guerlesquin F, Bruschi M. Biochimie. 1994; 76:471. [PubMed: 7880886]
12. Zu Y, Couture MMJ, Kolling DRJ, Crofts AR, Eltis LD, Fee JA, Hirst J. Biochemistry. 2003; 42:12400. [PubMed: 14567701]
13. Hunsicker-Wang LM, Heine A, Chen Y, Luna EP, Todaro T, Zhang YM, Williams PA, McRee DE, Hirst J, Stout CD, Fee JA. Biochemistry. 2003; 42:7303. [PubMed: 12809486]
14. Brown EN, Friemann R, Karlsson A, Parales JV, Couture MM, Eltis LD, Ramaswamy S. J Biol Inorg Chem. 2008; 13:1301. [PubMed: 18719951]
15. Zuris JA, Halim DA, Conian AR, Abresch EC, Nechushtai R, Paddock ML, Jennings PA. J Am Chem Soc. 2010; 132:13120. [PubMed: 20812736]
16. Yanagisawa S, Banfield MJ, Dennison C. Biochemistry. 2006; 45:8812. [PubMed: 16846224]
17. Varadarajan R, Zewert TE, Gray HB, Boxer SG. Science. 1989; 243:69. [PubMed: 2563171]
18. Shifman JM, Gibney BR, Sharp RE, Dutton PL. Biochemistry. 2000; 39:14813. [PubMed: 11101297]
19. Olea C Jr, Kuriyan J, Marletta MA. J Am Chem Soc. 2010; 132:12794. [PubMed: 20735135]
20. Johnson DC, Dean DR, Smith AD, Johnson MK. Annu Rev Biochem. 2005; 74:247. [PubMed: 15952888]
21. Fontecave M. Nat Chem Biol. 2006; 2:171. [PubMed: 16547473]
22. Mason JR, Cammack R. Annu Rev Microbiol. 1992; 46:277. [PubMed: 1444257]
23. Link TA. Adv Inorg Chem. 1999; 47:83.
24. Berry EA, Guergova-Kuras M, Huang LS, Crofts AR. Annu Rev Biochem. 2000; 69:1005. [PubMed: 10966481]
25. Cramer WA, Zhang H, Yan J, Kurisu G, Smith JL. Annu Rev Biochem. 2006; 75:769. [PubMed: 16756511]
26. Iwata S, Saynovits M, Link TA, Michel H. Structure. 1996; 4:567. [PubMed: 8736555]
27. Colbert CL, Couture MMJ, Eltis LD, Bolin J. Structure. 2000; 8:1267. [PubMed: 11188691]
28. Klingen AR, Ullmann GM. Biochemistry. 2004; 43:12383. [PubMed: 15449929]
29. Dikanov, SA. New Advances in Analytical Chemistry. Attaur-Rahman, editor. Gordon and Breach; Amsterdam: 2000. p. 523
30. Prisner T, Rohrer M, MacMillan F. Annu Rev Phys Chem. 2001; 52:279. [PubMed: 11326067]
31. Hoffman BM. Proc Natl Acad Sci USA. 2003; 100:3575. [PubMed: 12642664]
32. Dikanov SA, Shubin AA, Kounosu A, Iwasaki T, Samoilova RI. J Biol Inorg Chem. 2004; 9:753. [PubMed: 15243789]
33. Iwasaki T, Kounosu A, Uzawa T, Samoilova RI, Dikanov SA. J Am Chem Soc. 2004; 126:13902. [PubMed: 15506733]
34. Dikanov SA, Kolling DRJ, Endeward B, Samoilova RI, Prisner TF, Nair SK, Crofts AR. J Biol Chem. 2006; 281:27416. [PubMed: 16854984]

35. Iwasaki T, Samoilova RI, Kounosu A, Dikanov SA. FEBS Lett. 2009; 583:3467. [PubMed: 19804777]
36. Kounosu A, Li Z, Cosper NJ, Shokes JE, Scott RA, Imai T, Urushiyama A, Iwasaki T. J Biol Chem. 2004; 279:12519. [PubMed: 14726526]
37. Iwasaki T, Kounosu A, Tao Y, Li Z, Shokes JE, Cosper NJ, Imai T, Urushiyama A, Scott RA. J Biol Chem. 2005; 280:9129. [PubMed: 15632131]
38. Iwasaki T, Kounosu A, Kolling DRJ, Crofts AR, Dikanov SA, Jin A, Imai T, Urushiyama A. J Am Chem Soc. 2004; 126:4788. [PubMed: 15080677]
39. (a) Kounosu A, Hasegwa K, Iwasaki T, Kumasaka T. Acta Cryst Sect F. 2010; 66:842.(b) Hasegawa K, Urushiyama A, Miyajima-Nakano Y, Baldansuren A, Dikanov SA, Iwasaki T, Kumasaka T. in preparation for submission.
40. Lin MT, Sperling LJ, Frericks Schmidt HL, Tang M, Samoilova RI, Kumasaka T, Iwasaki T, Dikanov SA, Rienstra CM, Gennis RB. Methods. 2011; 55:370. [PubMed: 21925267]
41. Waugh DS. J Biomol NMR. 1996; 8:184. [PubMed: 8914274]
42. Datsenko KA, Wanner BL. Proc Natl Acad Sci USA. 2000; 97:6640. [PubMed: 10829079]
43. Cherepanov PP, Wackernagel W. Gene. 1995; 158:9. [PubMed: 7789817]
44. Iwasaki T, Samoilova RI, Kounosu A, Ohmori D, Dikanov SA. J Am Chem Soc. 2009; 131:13659. [PubMed: 19736979]
45. Stoll S, Calle G, Mitrikas G, Schweiger A. J Magn Reson. 2005; 177:93. [PubMed: 16112885]
46. Gurbiel RJ, Doan PE, Gassner GT, Macke TJ, Case DA, Ohnishi T, Fee JA, Ballou DP, Hoffman BM. Biochemistry. 1996; 35:7834. [PubMed: 8672484]
47. Dikanov SA, Samoilova RI, Kappl R, Crofts AR, Hüttermann J. Phys Chem Chem Phys. 2009; 11:6807. [PubMed: 19639155]
48. Dikanov SA, Tyryshkin AM, Bowman MK. J Magn Reson. 2000; 144:228. [PubMed: 10828191]

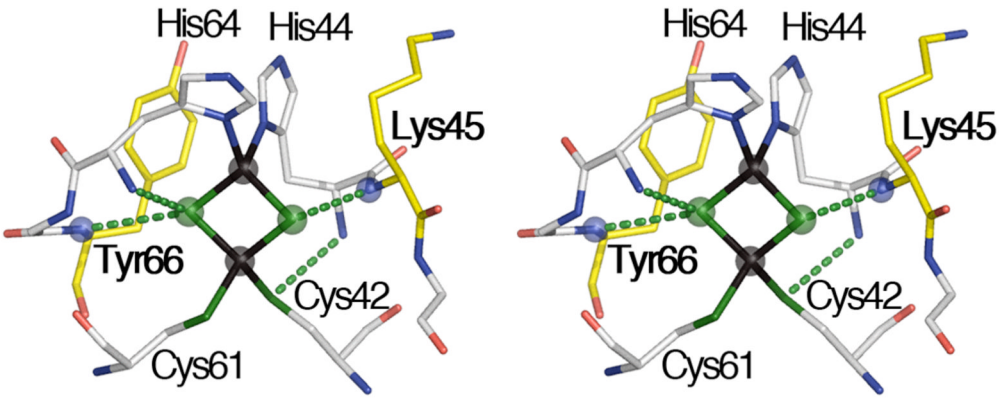

Figure 1.

The wall-eye stereoview of the possible hydrogen bond network around the low-potential Rieske-type [2Fe-2S](His)$_2$(Cys)$_2$ cluster (Fe as *dark-brown spheres* and bridging S (S^b) as *green spheres*) binding site in the ARF structure.[39b] Locations of Lys45 and Tyr66 (*yellow sticks*) and their peptide N_α atoms discussed in the text (*blue spheres*) are indicated.

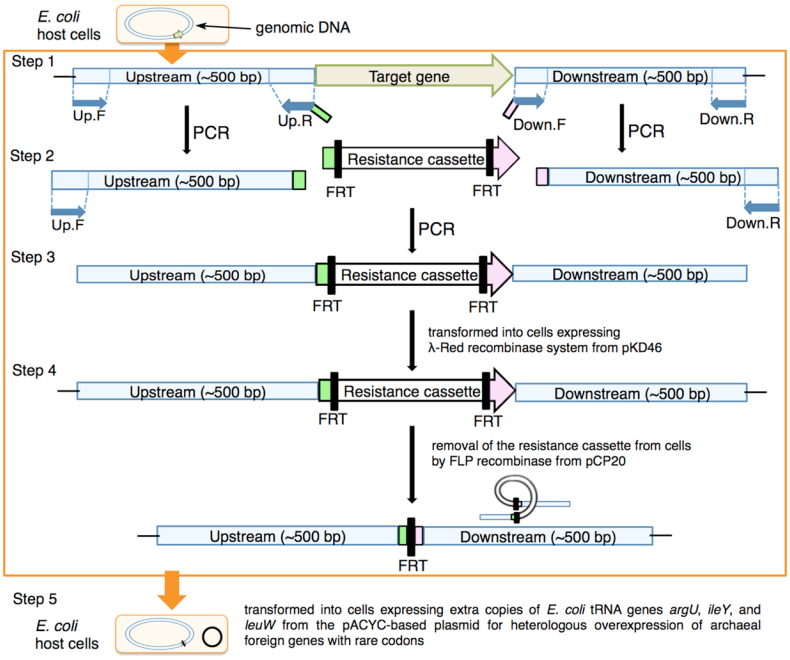

Figure 2.

Schematic procedures used for the deletion of a target chromosomal gene with the λ-Red recombination system[42] (steps 1–3).[40] In this work, the resistance cassette was removed from the new knock-out strain by FLP recombinase expressed from pCP20 vector[43] (step 4),[40] and a pACYC-based plasmid harboring tRNA genes (*argU*, *ileY*, and *leuW*) for the *E. coli* rare codons was subsequently incorporated into the resulting cells (step 5). FRT, FLP recombination target.[43]

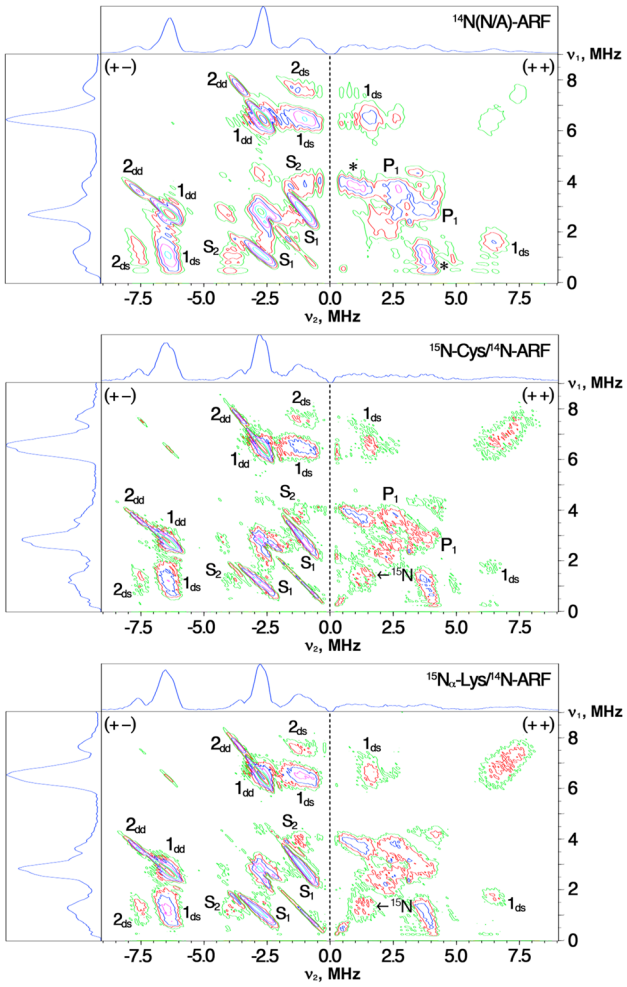

Figure 3.

HYSCORE spectra in contour presentation of the reduced ARF samples measured under the similar conditions at g_y=1.90 (363.4 mT for unlabeled (^{14}N(N/A)) ARF (control, *top*),[32] and 363.1 mT for ^{15}N-Cys (*middle*) and $^{15}N_\alpha$-Lys (*bottom*) labeled ARF samples on the ^{14}N(N/A)-protein background; **τ**=136 ns; 10 K). Note that the observed ^{15}N signals from the input ^{15}N amino acid are very weak and vague in both ^{15}N-Cys (*middle*) and $^{15}N_\alpha$-Lys (*bottom*) labeled samples on the ^{14}N(N/A)-protein background, because of the intense signals from the coordinating $^{14}N_{\delta(His)}1$ and $^{14}N_{\delta(His)}2$ in the Rieske-type protein system[32] that overshadowed and cross-suppressed the expected weakly coupled (non-coodinating) ^{15}N cross-peaks (*cf.*, see Figs. 4, 5). ^{14}N nucleus can theoretically produce up to 18 cross-peaks in the HYSCORE spectra including two [$dq_{\pm}$, $dq_{\mp}$], eight [$dq_{\pm}$, $sq^{(1,2)}{}_{\mp}$], and eight [$sq^{(1,2)}{}_{\pm}$, $sq^{(1,2)}{}_{\mp}$] correlations, although only some of possible cross-features are usually observed in the experimental spectra of iron-sulfur proteins.[32,44] 1_{dd}, 1_{ds} and 2_{dd}, 2_{ds} mark dq–dq and dq–sq transitions for the coordinating $^{14}N_{\delta(His)}1$ and $^{14}N_{\delta(His)}2$ of ARF, respectively.[32] The cross-peaks from $^{14}N_{\delta(His)}1$: (1_{dd}), [±6.5, ∓2.7] MHz; (1_{ds}), [±6.5, ∓1.1] MHz and [6.5, 1.6] MHz; (S1) and (S2), sq–sq correlations at [±2.8, ∓1.1] MHz and [±4.0, ∓1.1] MHz, respectively.[32] The cross-peaks from $^{14}N_{\delta(His)}2$: (2_{dd}), [±7.6, ∓3.5] MHz; (2_{ds}), [±7.6, ∓ 1.2–1.3] MHz.[32] Peaks $\mathbf{P_1}$[32]: assigned to be Lys45 N_α (N_p1) as described in the text. Peaks with asterisks: re-assigned to sq-sq correlations of the coordinating $^{14}N_{\delta(His)}$ in this work.

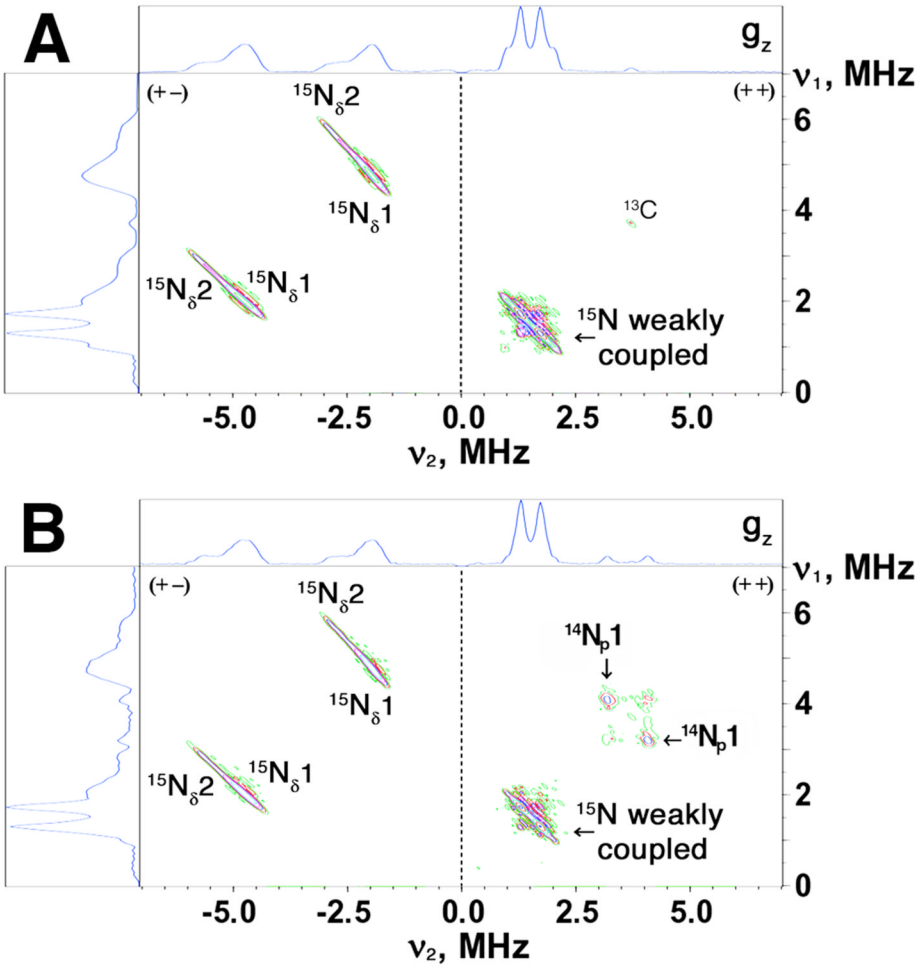

Figure 4.

HYSCORE spectra in contour presentation of the reduced Rieske-type cluster in selectively ^{14}N(N/A) L-tyrosine (**A**) and ^{14}N(N/A) L-lysine (**B**) labeled ARF on the ^{15}N-protein background, recorded at the g_z area (345.0 mT) of the EPR line (time τ=136 ns, 10 K). Because ^{15}N with nuclear spin I=1/2 has only two nuclear frequencies, each ^{15}N may produce only a single pair of the cross-features which are located symmetrically relative to the diagonal line in the (+−) or (++) quadrant of the HYSCORE spectrum (depending on the ^{15}N hyperfine coupling strength).[33–35]

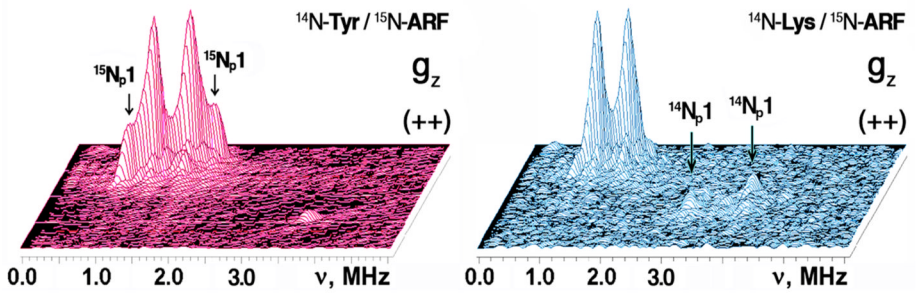

Figure 5.

3D presentation of the HYSCORE spectra in the (++) quadrant of ^{14}N(N/A) L-tyrosine (*left*) and ^{14}N(N/A) L-lysine (*right*) labeled ARF on the ^{15}N-protein background (recorded near g_z area at the same conditions as Fig. 4), showing the variation of the ^{15}N cross-feature lineshapes. The similar ^{15}N splittings were also observed at some intermediate positions between the low- and high-field edges (*e.g.*, see Fig. 6), indicating their predominantly isotropic characters. The largest splitting for $^{15}N_p1$ with the isotropic hyperfine coupling a=1.03 MHz (Table 2), resolved in the ^{14}N L-tyrosine labeled ARF (*left*), is missing in the ^{14}N L-lysine labeled protein (*right*).

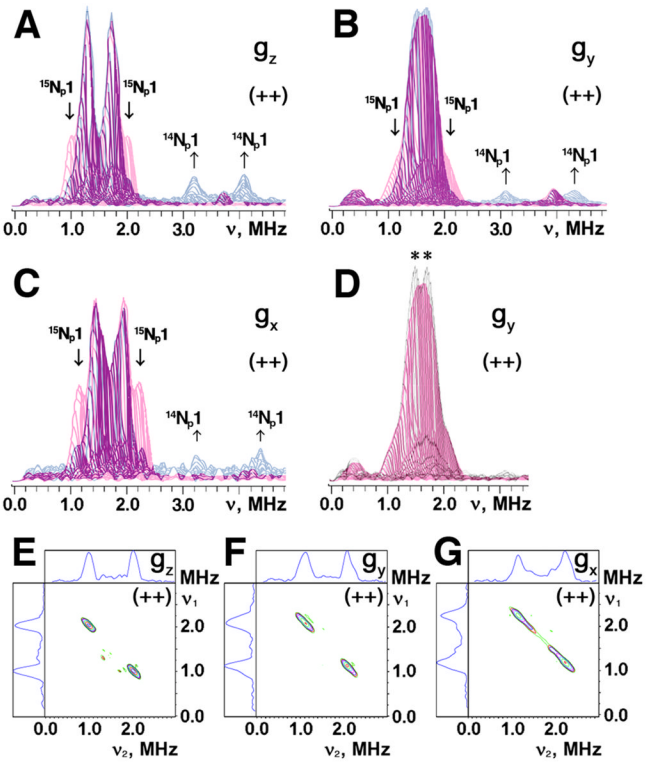

Figure 6.

Superimposed stacked HYSCORE spectra in the (++) quadrant of ^{14}N(N/A) L-tyrosine (*red*) and ^{14}N(N/A) L-lysine (*blue*) labeled ARF on the ^{15}N-protein background (**A–C**), and their ^{15}N difference (i.e. "^{14}N(N/A) L-tyrosine labeled ARF" *minus* "^{14}N(N/A) L-lysine labeled ARF") HYSCORE spectra for $^{15}N_p1$ cross-peaks in contour presentation (**E–G**), recorded near the g_z (**A,E**), g_y (**B,F**), and g_x (**C,G**) areas at 10 K. Contribution of $^{15}N_p1$ (with the isotropic hyperfine coupling a=1.03 MHz, Table 2) and $^{14}N_p1$ for L-lysine to the nitrogen ESEEM amplitude in the (++) quadrant is evident for ^{14}N L-tyrosine (*red*) and ^{14}N L-lysine (*blue*) labeled ARF, respectively, when the stacked spectra (with zero projection angles) were re-scaled and superimposed after normalizing the relative scales of the cross-peak intensities from two $N_{\delta(His)}$ ligands in the (+−) quadrant (**A–C**).[35] Similar approach was used to detect the possible contribution of ^{15}N L-tyrosine (with a narrow splitting of ~0.2 MHz) to the ^{15}N ESEEM amplitude in the (++) quadrant (marked with *asterisks* in (**D**)), when the stacked spectra of ^{14}N L-tyrosine (*red*) and uniformly ^{15}N-labeled[35] (*gray*) ARF (with zero projection angles) were re-scaled and superimposed after normalizing the relative scales of the $^{15}N_{\delta(His)}$ cross-peak intensities in the (+−) quadrant (**D**). The same small **τ**-value (**τ**=136 ns; slightly exceeding the dead time of the instrument) was chosen for the measurement of these HYSCORE spectra, which allows the preferable observation of the undistorted lineshape of the cross-peaks as well as the minimization of the suppression effect on the ESEEM amplitudes.[48] Magnetic field, and microwave frequency, respectively: 345.0 mT (near g_z), 9.695 GHz (**A,E**); 365.5 mT (near g_y), 9.695 GHz (**B,F**); 386.7 mT (near g_x), 9.695 GHz (**C,G**); 363.1 mT (near g_y), 9.695 GHz (**D**).

Table 1

New *E. coli* amino acid auxotroph host strains used for overexpression of foreign genes

Strain	Precursor strain	Genes deleted	Selective amino acid labeling	References
ML40K1[a]	C43(DE3)	*ilvE avtA aspC hisG argH metA lysA*	Ile, Val, His, Arg, Met, Lys, Leu,[b] Tyr[c]	Ref. [40]
YM154[a,d]	C43(DE3)	*cysE*	Cys	Unpublished[d]
RF3	BL21(DE3)	*aspC*	N.A.[e]	This work
RF4RIL[a]	BL21(DE3)	*aspC, tyrB*	Tyr, Phe	This work

[a]These strains can be used for overexpression of foreign genes with rare codons (Fig. 2, step 5).

[b]In the presence of 0.4–1 mM Tyr, *tyrB* is repressed and Leu is required for growth in minimal medium.[40] This strategy can only be applicable for a short-term cultivation but *not* suitable for a long-term cultivation for heterologous expression of foreign genes.

[c]In the presence of 0.4–1 mM Tyr, *tyrB* is repressed and Tyr is required for growth in minimal medium.[40] This strategy can only be applicable for a short-term cultivation but *not* suitable for a long-term cultivation for heterologous expression of foreign genes.

[d]C43(DE3) strain YM154 is a new cysteine auxotroph that grows normally in Luria-Bertani medium, but poorly in nonlabeled CHL medium with negligible amount of L-cysteine [to be published].

[e]Not applicable. BL21(DE3) strain RF3 is a precursor without any resistance cassette (Fig. 2, step 4) and was used for construction of the RF4RIL strain.

Table 2

Hyperfine couplings of weakly coupled ^{15}N nuclei currently resolved in the (++) quadrant of ^{15}N HYSCORE spectra of amino acid-specifically nitrogen labeled ARF samples.

Samples/assigned peaks	$^{15}A_z$ [a] (MHz)	$^{15}A_y$ [a] (MHz)	$^{15}A_x$ [a] (MHz)	^{15}a [b] (MHz)	$^{14}A_z$ [c] (MHz)	$^{14}A_y$ [c] (MHz)	$^{14}A_x$ [c] (MHz)	^{14}a [b] (MHz)	References
^{15}N-ARF (uniformly labeled)	1.03	~1.22[d]	1.1	~1.1[d]	0.74	~0.9[d]	0.8	~0.8[d]	Ref. [35]
	0.43	(0.25)[e]	0.49	-	0.3	(0.18)[e]	0.35	-	
^{14}N-Tyr/^{15}N-ARF[f]	1.04	N.R.[g]	1.12	-	0.74	N.R.[g]	0.80	-	This work
	0.43		0.49		0.3		0.35		
^{14}N-Lys/^{15}N-ARF[h, i]	0.43	(~0.25)[e]	0.49	-	0.3	(~0.18)[e]	0.35	-	This work
$^{15}N_p1$ (Lys45 N_α) peaks[j]	1.04	0.95	1.10	1.03	0.74	0.68	0.79	0.74	This work

[a] HYSCORE spectra recorded at the low- and high-field edges near the maximal and minimal g values give "single-crystal-like" patterns from the reduced Rieske-type cluster, whose g_z and g_x axes are directed along the external magnetic field. In contrast, the resonance condition at the intermediate g_y value is fulfilled by many different, yet well-defined orientations. ^{15}N hyperfine couplings ($^{15}A_i$ (i=z,y,x)) are based on a difference of two cross-peak coordinates described in the first-order by the equation: $\nu_{1,2} = |^{15}\nu_N \pm {}^{15}A_i/2|$. The positions of the peak maxima in the (++) quadrant were determined with the accuracy ~0.04 MHz.

[b] $A_i = a + T_{ii}$ (i=z,y,x), where a is an isotropic hyperfine coupling, and T_{ii} is an anisotropic hyperfine tensor component which is a diagonal component of the hyperfine tensor in the g-tensor coordinate system; $T_{xx}+T_{yy}+T_{zz}=0$ due to the tensor properties. Thus, $A_x+A_y+A_z=3a$ and $a=(A_z+A_y+A_x)/3$. The variations of the splittings at different g_i (i=z,y,x) suggest that the ^{15}T component of an anisotropic tensor ($-T,-T,2T$) has an order ~0.1–0.15 MHz (or ^{14}T ~ 0.07–0.11 MHz), in agreement with the previous considerations based on the point-dipole approximation model.[47] The tensor component would be larger for nitrogen nuclei located around the innermost Fe(III) side and smaller on the outermost Fe(II) side of the reduced [2Fe-2S] cluster. For the isotropic hyperfine couplings $^{14,15}a$, only the values for the largest splittings are given in this table.

[c] ^{14}N hyperfine couplings, $^{14}A_i$ (i=z,y,x), were recalculated from the corresponding $^{15}A_i$ (i=z,y,x) coupling values.

[d] These tentative $^{14,15}A_y$ and $^{14,15}a$ values were based on the total width of the ^{15}N HYSCORE spectrum recorded near g_y[35] and thus probably overestimated.

[e] A very narrow splitting in the (++) quadrant (see Fig. 6B,D).

[f] The ^{15}N cross-peaks resolved in the (++) quadrant: [2.03, 0.99] and [1.73, 1.30] MHz near g_z; [2.27, 1.15] and [1.94, 1.45] MHz near g_x (see Figs. 5,6).

[g] Not resolved (see Fig. 6B).

[h] The ^{15}N cross-peaks resolved in the (++) quadrant: [1.73, 1.30] MHz near g_z, and [1.94, 1.45] MHz near g_x.

[i] The ^{14}N cross-peaks ($^{14}N_p1$) resolved in the (++) quadrant in this sample (see Figs. 4B, 6A,C): [4.08, 3.19] MHz near g_z and [4.41, 3.34] MHz near g_x, which gave the (tentative) ^{14}N hyperfine couplings $^{14}A_z$ of 0.76 MHz near g_z and $^{14}A_x$ of 0.87 MHz near g_x, respectively, as estimated using formal expressions for the double-quantum (dq) transitions in the powder-type spectrum, $\nu_{dq\pm} = 2[(^{14}\nu_N \pm {}^{14}A_i/2)2 + K^2 (3 + \eta^2)]^{1/2}$, where K is a nuclear quadrupole coupling constant and η is an asymmetry parameter.

[j] The $^{15}N_p1$ cross-peaks were well-resolved in the difference HYSCORE spectra in the (++) quadrant (see Fig. 6E–G): [2.03, 0.99] MHz near g_z, [2.02, 1.12] MHz near g_y, and [2.24, 1.14] MHz near g_x.